Second Coordination Sphere Effect Shifts CO 2 to CO Reduction by Iron Porphyrin from Fe 0 to Fe I

Sk Amanullah, Philipp Gotico, Marie Sircoglou, Winfried Leibl, Manuel Llansola-Portoles, Tania Tibiletti, Annamaria Quaranta, Zakaria Halime, Ally Aukauloo

RESEARCH ARTICLE

Second Coordination Sphere Effect Shifts CO_2 to CO Reduction by Iron Porphyrin from Fe^0 to Fe^I

Sk Amanullah,* [a,b] Philipp Gotico,[b] Marie Sircoglou,[a] Winfried Leibl,[b] Manuel J. Llansola-Portoles,[b] Tania Tibiletti,[b] Annamaria Quaranta, [b] Zakaria Halime,*[a] and Ally Aukauloo,*[a,b]

[a] Dr. S. Amanullah, Dr. Marie Sircoglou, Dr. Z. Halime, Prof. A. Aukauloo
Université Paris-Saclay, CNRS, Institut de Chimie Moléculaire et des Matériaux d'Orsay, 91400, Orsay, France.
E-mail: amanullah.sk@cea.fr, zakaria.halime@universite-paris-saclay.fr, ally.aukauloo@universite-paris-saclay.fr

[b] Dr. S. Amanullah, Dr. P. Gotico, Dr. W. Leibl, Dr. M. J. Llansola-Portoles, Dr. T. Tibiletti, Dr. A. Quaranta, Prof. A. Aukauloo
Université Paris-Saclay, CEA, CNRS, Institute for Integrative Biology of the Cell (I2BC), 91198, Gif-sur-Yvette, France.

Supporting information for this article is given via a link at the end of the document.

Abstract: Iron porphyrins are among the most studied molecular catalysts for carbon dioxide (CO_2) reduction and their reactivity is constantly being enhanced through the implementation of chemical functionalities in the second coordination sphere inspired by the active sites of enzymes. In this study, we were intrigued to observe that a multipoint hydrogen bonding scheme provided by embarked urea groups could also shift the redox activation step of CO_2 from the well-admitted Fe(0) to the Fe(I) state. Using EPR, resonance Raman, IR and UV-Visible spectroscopies, we underpinned a two-electron activation step of CO_2 starting from the Fe(I) oxidation state to form, after protonation, an Fe(III)–COOH species. The addition of another electron and a proton to the latter species converged to the cleavage of a C–O bond with the loss of water molecule resulting in an Fe(II)–CO species. The DFT analyses of these postulated intermediates is in good agreement with our collected spectroscopic data, thus allowing us to propose an alternative pathway in the catalytic CO_2 reduction with iron porphyrin catalyst. Such a remarkable shift opens new lines of research in the design of molecular catalysts to reach low overpotentials in performing multi-electronic CO_2 reduction catalysis.

Introduction

Nature uses sunlight to fix carbon dioxide (CO_2) from our atmosphere to form energy-rich reduced hydrocarbons.[1-2] The massive scale of anthropogenic CO_2 emission due to the extensive use of fossil fuels has overwhelmed the natural pathways of CO_2 regulation in our biosphere.[3-4] Currently, a major concern for scientists is to discover new ways to return the highly stable CO_2 molecule to carbon-based fuels or synthetic chemicals commodities at a rate nearing its production.[5-10] We are far from reaching this target! To date, no economical solution is yet available on a global scale to perform these conversions. This is primarily because of the need of expensive and rare materials as catalysts and the high energy inputs required as compared to the thermodynamics.[11] The reduction of CO_2 also faces an unsolved issue, *i.e.,* the selectivity of the reduced forms of carbon.[12-13] This is an important aspect to consider as it will impact the development of the accompanying technologies accordingly, be it a gas or liquid form.[14-15] A current subject of intense investigation concerns the quest for molecular catalysts that borrow chemical principles from enzymes involved in the transformation of CO_2 to reach unmatched reactivity and selectivity.[16-22]

We have recently witnessed a noticeable advancement in the design of various molecular catalysts to realize the electro- and/or photo-catalytic CO_2 reduction.[23-28] Among these, metalloporphyrins are ranged in the most active systems for the formation of CO or HCOOH. Although CO is only a two-electron reduced form of CO_2, it is the starting point for the syngas process and thus may contribute in different ways to mitigate the anthropogenic CO_2 production. The synthesis of designed porphyrins holding functions that can play roles of proton relay, hydrogen bonding, and local electrostatic units with respect to the capture of CO_2 and stabilization of fugacious intermediates, has been beneficial to boost the kinetics of the reaction.[6, 8, 29] In particular, a constant focus of molecular chemists is to shift the required overpotential for CO_2 reduction to lower values. While this can be achieved with the addition of electron withdrawing groups, the deceiving counterpart of these results is a drastic fall in the kinetics of the reaction due to a decreased nucleophilic character of the formal Fe(0) active species.

Recently, we have shown that the presence of urea groups through a multipoint hydrogen bonding scheme helped in the capture and activation of CO_2 while shifting the overpotential to lower values and maintaining a high turnover frequency.[30-31] In a subsequent study, we have reported that upon photocatalysis of such urea-substituted porphyrin (**UrFe)** catalyst (Figure 1), the Fe(I) species was found to be the active species for CO_2 activation instead of the commonly accepted Fe(0) species.[32] This finding has urged us to investigate in further detail the electrochemical and chemical activation of CO_2 with this family of iron porphyrin catalysts. Herein, we describe that the Fe(I) (**$UrFe^I$)** species is already sharing two electrons with the CO_2 substrate to form a transient Fe(III)–COO(H) species. All the gathered resonance Raman, infrared (IR), ultraviolet-visible (UV-Vis) and electron paramagnetic resonance (EPR) spectroscopic data are supportive for this activation process.

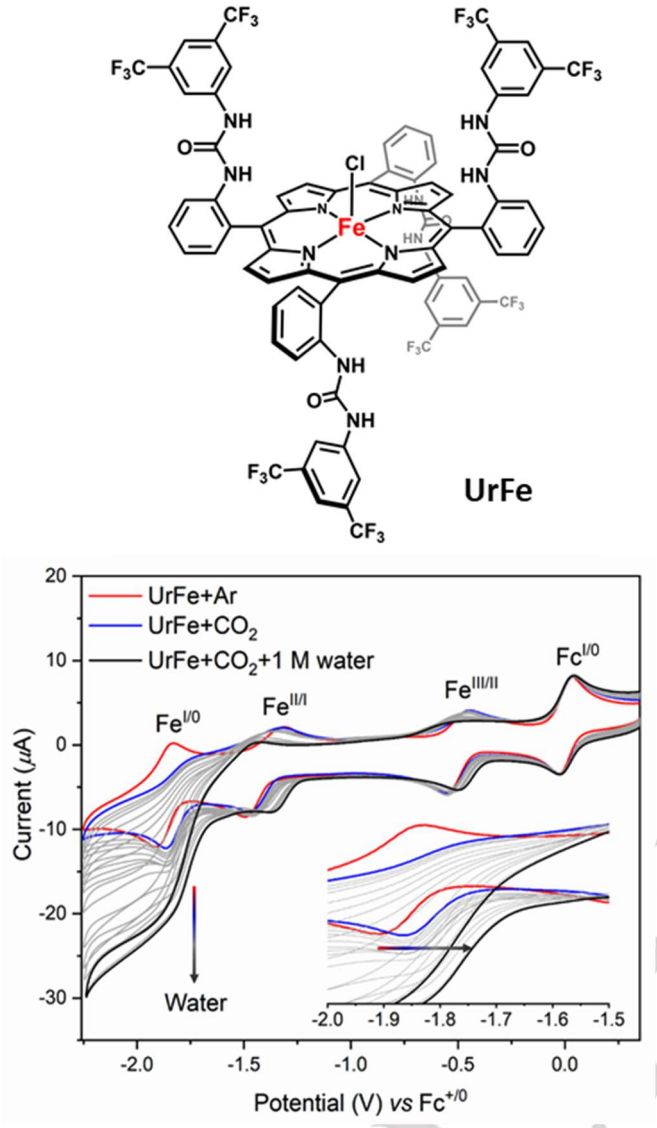

Figure 1. Chemical structure of **UrFe** catalyst (top). Cyclic voltammograms of **UrFe** (bottom) under argon saturation (red), CO_2 saturation (blue), and an increasing amount of water (grey to black). A zoom on the –1.5 to –2.0 V region is given as inset. Voltammograms were recorded at 0.1 Vs^{-1} in ACN:DMF (5:1, 0.5 mM catalyst concentration) with 0.1 M $[Bu_4N]PF_6$ supporting electrolyte, a saturated calomel (SCE) reference electrode, Platinum counter electrode and glassy carbon working electrode. Ferrocene was added as an internal reference.

As such, these results show for the first time that manipulating the second coordination sphere can shift the redox activation of CO_2 at an iron porphyrin from an Fe(0) to an Fe(I) oxidation state in a homogeneous medium. Such a finding opens a new paradigm in molecular catalysis for CO_2 reduction on the way to push the overpotential to lower values.

Results and Discussion

Electrocatalytic reduction of CO_2 by UrFe catalyst

The electrochemical study of **UrFe** catalytic performances has shown that the multipoint hydrogen bonding network provided by the urea groups in the second coordination sphere of the iron center can decrease the catalytic overpotential ($\eta = E^0_{cat} - E^0_{CO2/CO}$) while maintaining a higher turnover frequency (TOF).[30] In an argon (Ar) degassed acetonitrile (ACN):dimethylformamide (DMF)/ 5:1 solution containing 0.1 M of tetra-*N*-butylammonium hexafluorophosphate ($[Bu_4N]PF_6$), the cyclic voltammograms of **UrFe**, as well as its nonfunctionalized analogue (**TPPFe**), display three reversible redox waves corresponding respectively to the formal $Fe^{III/II}$, $Fe^{II/I}$, $Fe^{I/0}$ redox couples (Figure 1, Figure S1 and Table S1). In the case of **UrFe**, there is a noticeable shift towards more positive potentials due to the electron withdrawing effect of the urea arms. Under a CO_2 atmosphere and in presence of water as a proton source, an important catalytic current can be observed on the third reduction wave for both catalysts which corresponds to the 2-electron reduction of CO_2 to CO. Besides the 300 mV gain in the overpotential (η(**TPPFe**) = 0.73 V *vs* η(**UrFe**) = 0.43 V) and comparable reaction rate ($\log TOF_{max}$(**TPPFe**) = 4.03 *vs* $\log TOF_{max}$(**UrFe**) = 3.83) determined using Foot of the Wave Analysis,[30] an intriguing observation is that, unlike **TPPFe**, **UrFe** displays a clear positive shift of the last reduction wave ($Fe^{I/0}$) when switching from Ar to CO_2 atmosphere. In presence of water, the catalytic process seems to proceed at a significantly more positive potential than the $Fe^{I/0}$ redox potential (Figure 1). It should be noted that, in absence of CO_2, water has no significant effect on the $Fe^{I/0}$ redox potential (Figure S2). The question that raises then is: can CO_2 be activated and reduced by **UrFe** already at the Fe^{I} oxidation state? A previous photocatalytic study has shown that, due to the multipoint hydrogen bonding interactions in the second sphere, CO_2 can be activated at Fe^{I} oxidation state but no catalytic formation of CO can be observed at this oxidation state.[32]

To interrogate the ability of **UrFe^{I}** to activate and reduce CO_2, *in-situ* Fourier Transform Infrared SpectroElectroChemistry (FTIR-SEC) experiments were performed during a controlled potential electrolysis (CPE) at –1.55 *vs* $Fc^{+/0}$, a potential just negative enough to generate the **UrFe^{I}** intermediate in presence of CO_2 and water. Although no CO evolution can be detected by gas chromatography (GC) analysis of the reaction headspace, a strong C=O vibration at 1958 cm^{-1} was observed with a shift to 1915 cm^{-1} when using $^{13}CO_2$ (Figure 2). This C=O vibration is characteristic of a **UrFe^{II}–CO** species that can also be easily prepared by purging CO into a **UrFe^{II}** solution obtained by reducing **UrFe^{III}Cl** on Zinc-amalgam, Zn(Hg).[33-34] It appears therefore that at this potential, CO_2 undergoes a single turnover reduction to yield a **UrFe^{II}–CO** species. Interestingly, CO starts to be catalytically produced when a potential more negative than –1.67 V *vs* $Fc^{+/0}$ is applied (Figure S3). Of note, this potential is slightly more negative than that of the Fe^{II}–CO reduction peak (–1.65 V *vs* $Fc^{+/0}$, Figure S4, Table S1) but it is not reducing enough to generate the **UrFe^{0}** oxidation state (the onset potential of the $UrFe^{I/0}$ cathodic wave is located at –1.79 V *vs* $Fc^{+/0}$) reported to be the active species in CO_2 reduction by iron porphyrins.[35] This implies that CO_2 binding and activation proceeds already with **UrFe^{I}** at the most positive potential ($E_{½}(UrFe^{II/I})$ = –1.40 V *vs* $Fc^{+/0}$) ever reported for CO_2 activation by an iron-porphyrin. In our

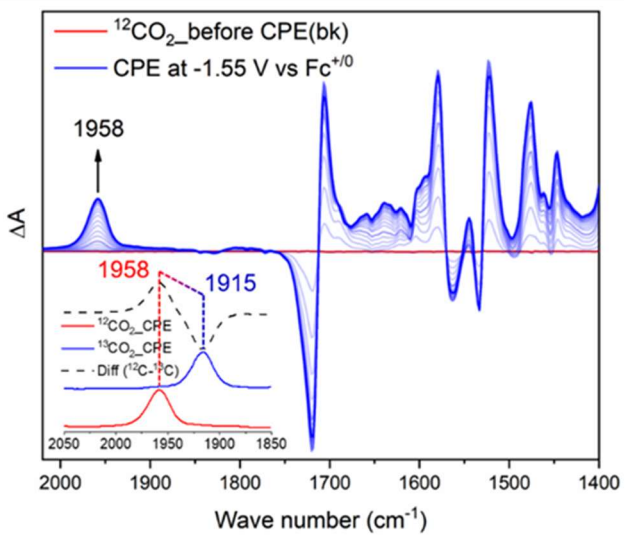

Figure 2. FTIR-SEC differential spectra of **UrFe** in CO_2 saturated deuterated acetonitrile (4 mM catalyst concentration) in presence of 0.1 M $[Bu_4N]PF_6$ supporting electrolyte, Ag-wire pseudo-reference electrode and Platinum mesh as both counter and working electrodes. Background was collected before applying the potential (red). Controlled potential electrolysis was performed at –1.55 V *vs* $Fc^{+/0}$ (blue traces). Inset: 1958 cm^{-1} (red) vibrational band corresponding to C=O stretching frequency shifts to 1915 cm^{-1} (blue) when replacing $^{12}CO_2$ with $^{13}CO_2$

pervious photocatalytic study, we demonstrated that this early activation by the less nucleophilic Fe(I) center results from the Fe(I)–CO_2 adduct stabilization by the quadruple hydrogen bonds, placing it only 0.78 kcal.mol^{-1} higher than the dissociated pair. This energy difference corresponds to an association constant of ca. 1 M. In contrast, a perfluorinated FeTPP with similar redox potentials displays an association constant as low as 10^{-8} M, rendering CO_2 binding to Fe(I) species highly unlikely. It is noteworthy that Dey and co-workers recently reported that an Fe(I)-chlorin, a doubly reduced form of a porphyrin, holding a pendant amine as proton relay, was also able to activate CO_2.[36] Hoverer, in absence of the hydrogen bonding stylization, CO_2 binding to Fe(I) was only feasible due to the more pronounced nucleophilic character of this species generated at 180 mV more negative potential than that required for **UrFe^{I}**. Moreover, in sharp contrast with the commonly observed CO formation with iron-porphyrin catalysts, Fe(I)-chlorin sees to follow a different reaction mechanism leading to an exclusive formation of HCOOH. To better understand the original reactivity observed for CO_2-to-CO catalytic electroreduction by **UrFe**, we chemically generated the **UrFe^{I}** species and studied its reactivity toward CO_2.

UrFe^{I} reactivity towards CO_2

Decamethylcobaltocene ($CoCp_2^*$) was found to be an appropriate chemical reducing agent to form a pure formal Fe^{I} oxidation state (Figure S5-S8). At room temperature, the reaction of **UrFe^{I}** with CO_2 appears to be too fast to allow the detection of any intermediate by UV-Vis absorption spectroscopy. However, when the reaction is performed in dry butyronitrile at –75 °C, just above the sublimation point of CO_2, the characteristic Soret band of **UrFe^{I}** at 446 nm quickly disappears giving rise to a new Soret band at 440 nm (Figure 3a). The intermediate corresponding to this Soret band then slowly decays within 10 min to evolve to a new species with a maximum absorption at 430 nm. Interestingly, when the same reaction is performed in presence of 5 mM of water (Figure 3b), only this last species can be observed which leads us to assume that, even though a dry solvent was used in the initial experiment (see solvent drying procedure in the SI), the CO_2 adduct first formed with **UrFe^{I}** displaying a Soret band at 440 nm, undergoes a protonation process to form a new species with a Soret band at 430 nm.

To investigate further the oxidation and spin states of these two intermediates, EPR spectroscopy was also employed. The spectrum in the perpendicular X-band mode of a chemically generated **UrFe^{I}** at 15 K in butyronitrile exhibits three signals with g- values of 2.51, 2.26 and 1.93 (Figure 3c, red and Figure S6), **Figure 3.** a-b) UV-Vis absorption spectral changes after the addition of CO_2 gas into 10 μM **UrFe^{I}** solution in butyronitrile at a scan rate of 4800 nm/min and a temperature of –75 °C. c) X-band EPR spectra collected on frozen-glass samples of 1 mM **UrFe^{I}** solution in butyronitrile (red) in presence of CO_2 (green) and in presence of CO_2 and 5 mM of water (blue) at 15 K, 25 dB attenuation and 25 G modulation amplitude. d-f) Resonance Raman spectra collected with the frozen-glass samples at 77 K generated from 1 mM solution of **UrFe^{I}** in butyronitrile (red) in presence of CO_2 (green) and in presence of CO_2 and water (blue) at −75 °C.similar to those previously reported by Bocian *et al* for an Fe(I)-porphyrin with electron withdrawing groups.[37] Upon bubbling CO_2 in a **UrFe^{I}** solution for 30 s at –75 °C, a mixture of both rhombic low-spin ferric (g-values of 2.29, 2.17 and 1.95, Figure 3c, blue and inset) and high-spin ferric (g-values of 5.99 and 1.99, Figure 3c, green) species were generated. In a different experiment, using the CO_2-saturated **UrFe^{I}** stock solution with 5 mM of water, only the high-spin ferric species was generated (Figure 3c, blue). By combining the results of UV-Vis and EPR experiments, we can assume that the CO_2 adduct formed first with **UrFe^{I}** in dry solvent is a **[UrFe^{III}–CO_2]$^{-}$** intermediate and the species observed in presence of water is its protonated form formulated as **UrFe^{III}–CO_2H** (Scheme 1). The fact that this last protonated form can be observed even in a relatively dry solvent can be rationalized by the previously reported ability of urea groups to trap and activate water or bicarbonate as a proton source.[30, 38] The pK_a computed for this couple is very close to the reported acidity constant of ACN/water/CO_2 mixtures.[39] The observed change from a low-spin **[UrFe^{III}–CO_2]$^{-}$** to a high-spin **UrFe^{III}–CO_2H** species can be explained by a weakening in the electrostatic interaction between the Fe^{III} center and the carboxylate upon protonation, in agreement with the Fe–C distance increase from 1.96 to 2.16 Å noticed in the corresponding DFT-optimized structures (Scheme 1).

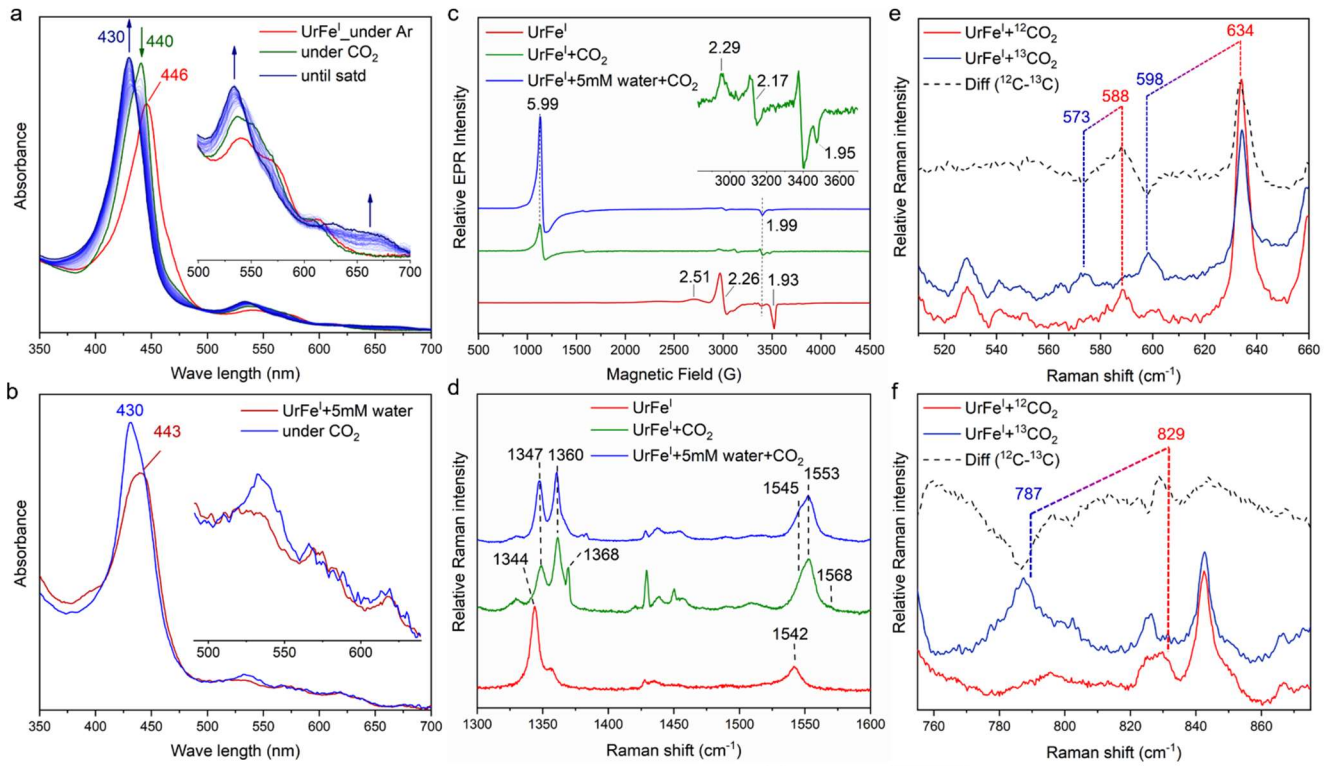

Figure 3. a-b) UV-Vis absorption spectral changes after the addition of CO_2 gas into 10 μM **UrFe^{I}** solution in butyronitrile at a scan rate of 4800 nm/min and a temperature of –75 °C. c) X-band EPR spectra collected on frozen-glass samples of 1 mM **UrFe^{I}** solution in butyronitrile (red) in presence of CO_2 (green) and in presence of CO_2 and 5 mM of water (blue) at 15 K, 25 dB attenuation and 25 G modulation amplitude. d-f) Resonance Raman spectra collected with the frozen-glass samples at 77 K generated from 1 mM solution of **UrFe^{I}** in butyronitrile (red) in presence of CO_2 (green) and in presence of CO_2 and water (blue) at −75 °C.

To further confirm the oxidation and spin states of the two intermediates, resonance Raman (rR) spectroscopy was employed because, in addition to its higher sensitivity, it has also well-established marker bands for iron porphyrins.[40] Laser providing excitation wavelength (441.6 nm) in the Soret band region of the intermediates was used to enhance the rR signals. First, the oxidation-state (ν_4) and spin-state (ν_2) marker bands for the **UrFe^{III}** resting state and the chemically reduced **UrFe^{II}** and **UrFe^{I}** were determined in butyronitrile at 77 K (Figure S7). It is worth mentioning that the ν_4 and ν_2 marker bands at 1344 cm^{-1} and 1542 cm^{-1}, respectively, corresponding to **UrFe^{I}** are in line with the recent electronic structure description for the formal Fe(I)-porphyrins as an Fe(II)-porphyrin-anion-radical from the groups of F. Neese and S. P. de Visser.[41-42] Upon CO_2 bubbling into an **UrFe^{I}** solution at –75 °C, three sets of ν_4 and ν_2 marker bands appeared at [ν_4 = 1368 cm^{-1} and ν_2 = 1568 cm^{-1}], [ν_4 = 1360 cm^{-1} and ν_2 = 1553 cm^{-1}] and [ν_4 = 1347 cm^{-1} and ν_2 = 1545 cm^{-1}] (Figure 3d). The first set of signals is typical of a low-spin ferric porphyrin and the second is characteristic of a high-spin ferric porphyrin.[40]

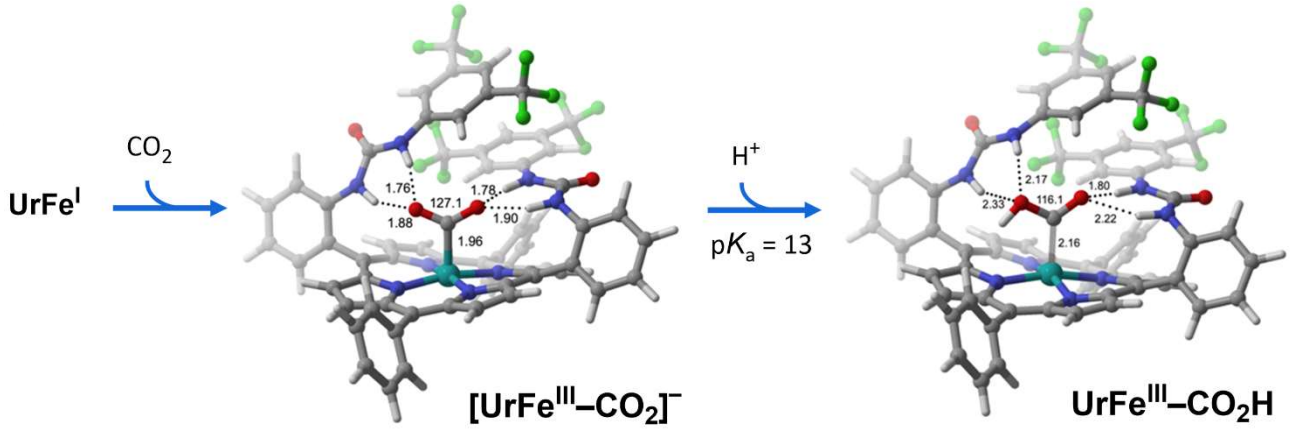

Scheme 1. Reactivity of **UrFe^{I}** towards CO_2 and DFT optimized geometries of **[Fe^{III}–CO_2]$^{-}$** and **Fe^{III}–CO_2H** intermediates.

Based on the UV-Vis and EPR experiments discussed earlier, these two sets of signals correspond respectively to **[UrFe^{III}–CO$_2$]$^-$** and **UrFe^{III}–CO$_2$H** because here also, in presence of water, the signals attributed to **[UrFe^{III}–CO$_2$]$^-$** disappeared in favor of those of **UrFe^{III}–CO$_2$H**. Using $^{13}CO_2$, two more isotope-sensitive bands corresponding to Fe–C and C–O bonds vibrations were identified for each intermediate (Figure 3e, 3f and Figure S8). **[UrFe^{III}–CO$_2$]$^-$** displays ν_{Fe-C} = 634 cm^{-1} and ν_{C-O} = 829 cm^{-1} that shift respectively to ν_{Fe-C} = 598 cm^{-1} and ν_{C-O} = 787 cm^{-1} when ^{13}C-labeled CO_2 is used, while **UrFe^{III}–CO$_2$H** has ν_{Fe-C} = 588 cm^{-1} and ν_{C-OH} = 1208 cm^{-1} that shift respectively to ν_{Fe-C} = 573 cm^{-1} and ν_{C-O} = 1177 cm^{-1}. Interestingly, when D_2O was used instead of H_2O, the ν_{C-OH} vibration band of **UrFe^{III}–CO$_2$H** at 1208 cm^{-1} was replaced by a new band at 1092 cm^{-1} (Figure S8b), giving thus more support to the proposed formulation of this intermediate. The assignment of the above mentioned rR vibration modes were made by supposing that they are similar to those observed for the iron-chlorin-based CO2 adducts reported by Dey and coworkers,[36, 43] and the analysis of the computed vibrational modes of model complexes optimized by DFT (Scheme 1 and Table S2).

The third set of signals is different from an eventual unreacted **UrFe^{I}** and rather corresponds to a high-spin ferrous species. The only species that can fit with this electronic description at this stage of the reaction is **[UrFe^{II}–CO$_2$H]$^-$** resulting from the one-electron-reduction of **UrFe^{III}–CO$_2$H**. Its formation results from the difficulty to have a perfect stoichiometry control during the preparation of **UrFe^{I}** samples (Figure S9), and hence the presence of a small excess of $CoCp_2$* (–1.98 V *vs* Fc$^{+/0}$) able to further reduce the **UrFe^{III}–CO$_2$H** intermediate. The potential of the **UrFe^{III}–CO$_2$H/[UrFe^{II}–CO$_2$H]$^-$** redox couple was indeed located at –1.05 V *vs* Fc$^{+/0}$ (Figure S10) and is more positive than that needed to generate **UrFe^{I}** (–1.44 V *vs* Fc$^{+/0}$). To confirm this hypothesis, the reactivity of **[UrFe^{III}–CO$_2$H]** in presence of a one-electron donor was studied in the following section.

UrFe^{III}–CO$_2$H Intermediate reactivity

Given the moderately negative potential required to reduce **UrFe^{III}–CO$_2$H** species, $CoCp_2$* was replaced in this section by the nonfunctionalized cobaltocene ($CoCp_2$) with less reducing power (–1.33 V *vs* Fc$^{+/0}$).

UV-Vis monitoring of the addition of one equivalent of $CoCp_2$ to a solution of **UrFe^{III}–CO$_2$H** shows the formation of a new species with a maximum absorption at 439 nm (Figure 4a).

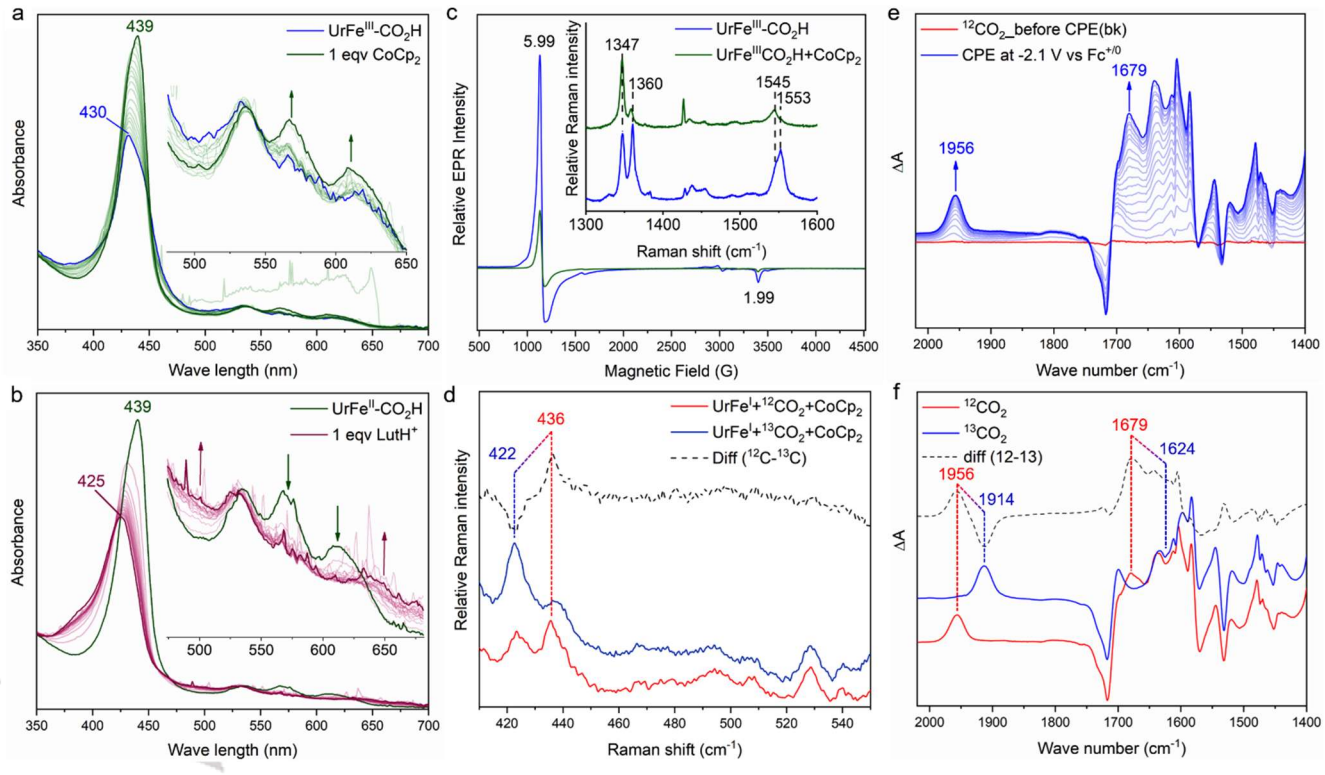

Figure 4. a-b) UV-Vis absorption spectral changes after the addition of $CoCp_2$ (a) and 2,6-Lutidinium triflate (b) on 10 μM **UrFe^{III}–CO$_2$H** solution at −75 °C. c) X-band EPR spectral changes at 15 K after the addition of $CoCp_2$ to a 1 mM solution of **UrFe^{III}–CO$_2$H** generated at −75 °C. The inset figure represents the resonance Raman spectral changes collected on frozen-glass samples at 77 K of 1 mM solution of **UrFe^{III}–CO$_2$H** in butyronitrile before (blue) and after the addition of $CoCp_2$ at −75 °C (green). d) Resonance Raman spectral collected on frozen-glass samples at 77 K of 1 mM solution of **[UrFe^{II}–CO$_2$H]$^-$** prepared at −75 °C using $^{12}CO_2$ (red) and $^{13}CO_2$ (blue) and their difference spectrum (black dash). e) FTIR-SEC spectra of **UrFe** in CO_2 saturated deuterated acetonitrile (4 mM catalyst concentration) with 0.1 M $[Bu_4N]PF_6$ supporting electrolyte, Ag-wire pseudo-reference electrode, and Pt mesh as both counter and working electrodes. Background was collected before applying the potential (red). Controlled potential electrolysis was performed at –2.1 V *vs* Fc$^{+/0}$ (blue traces). f) Difference spectrum of FTIR-SEC. 1956 cm^{-1} and 1679 cm^{-1} vibrational bands corresponding to C=O stretching frequencies shift to 1914 cm^{-1} and 1624 cm^{-1}, respectively, replacing $^{12}CO_2$ (red) with $^{13}CO_2$ (blue)

The Soret band at 439 nm could be associated with the one-electron-reduced high-spin ferrous species **[UrFe^{II}–CO$_2$H]$^-$** observed earlier by rR, and preceding the last protonation step that leads to C–O bond cleavage and the release of a water molecule to form **Fe^{II}–CO**. Confirmation of this scenario comes from the addition of one equivalent of 2,6-lutidinium as a proton source to this new species, resulting in an exclusive conversion to **Fe^{II}–CO** with a characteristic Soret band at 425 nm (Figure 4b). This last species can also be prepared directly by bubbling CO into a **UrFe^{II}** solution (Figure S11).

Going back to rR, **[UrFe^{II}-CO$_2$H]$^-$** (ν_4 = 1347 cm^{-1} and ν_2 = 1545 cm^{-1}), observed initially as a side product during the preparation of **UrFe^{III}–CO$_2$H** due to the presence of a small excess $CoCp_2^*$ (Figure 3d), can be directly prepared by adding one equivalent of $CoCp_2$ after bubbling CO_2 into a solution of **UrFe^{I}** (Figure 4c, inset). The isotope-sensitive vibrations ν_{Fe-C} = 436 cm^{-1} / 422 cm^{-1} ($^{13}CO_2$) (Figure 4d), ν_{C-OH} = 1109 cm^{-1} / 1070 cm^{-1} ($^{13}CO_2$) / 1029 cm^{-1} (D_2O) (Figure S8) and $\nu_{C=O}$ = 1679 cm^{-1} / 1624 cm^{-1} ($^{13}CO_2$, obtained from the *in-situ* FTIR-SEC during the CPE at –2.1 V *vs* Fc$^{+/0}$, Figures 4e-4f) were also identified for **[UrFe^{II}–CO$_2$H]$^-$** intermediate. The one-electron reduction of **UrFe^{III}–CO$_2$H** was also well-evidenced by EPR spectroscopy showing a decrease in its axial high-spin ferric signal (g-values of 5.99 and 1.99) upon the addition of a stoichiometric amount of $CoCp_2$ indicating the formation of the EPR silent **[UrFe^{II}–CO$_2$H]$^-$** (Figure 4c).

Reaction mechanism

By combining all information gathered from UV-Vis, FTIR, EPR and rR spectroscopies, we can propose a mechanism for the unprecedented electrocatalytic reduction of CO_2 by **UrFe** catalyst at a potential more positive than that needed to reach the formal Fe^0 oxidation state (Scheme 2). At –1.55 V *vs* Fc$^{+/0}$, the **UrFe^{I}** active species can be generated from the **UrFe^{III}** resting state by two successive one-electron transfers. The urea groups in the second coordination sphere then come into action by participating to an early CO_2 capture and activation, already at formal Fe^{I} oxidation state, through a multipoint hydrogen bonding interaction. The resulting CO_2 adduct is formulated as ferric low-spin **[UrFe^{III}–CO$_2$]$^-$** species based on EPR spectroscopy with g-values of 2.29, 2.17 and 1.95, along with rR marker bands at ν_4 = 1368 cm^{-1}, ν_2 = 1568 cm^{-1}, ν_{Fe-C} = 634 cm^{-1} and ν_{C-O} = 829 cm^{-1}, and UV-Vis absorption maximum at 440 nm. In the next step, **[UrFe^{III}–CO$_2$]$^-$** (pK_a = 13) undergoes protonation even in relatively dry organic solvent to yield a high-spin **UrFe^{III}–CO$_2$H** intermediate. This latter species displays a Soret absorption band at 430 nm, EPR signals with g-values of 5.99 and 1.99, and rR marker bands at ν_4 = 1360 cm^{-1}, ν_2 = 1553 cm^{-1}, ν_{Fe-C} = 588 cm^{-1} and ν_{C-OH} = 1208 cm^{-1}. Cyclic voltammetry experiments revealed that the reduction potential of **UrFe^{III}–CO$_2$H** (–1.05 V *vs* Fc$^{+/0}$) is more positive than that needed to generate the **UrFe^{I}** ($E_{½}$ **UrFe$^{II/I}$** = –1.40 V *vs* Fc$^{+/0}$).[39] Accordingly, **UrFe^{III}–CO$_2$H** is reduced in the next step to form a high-spin **[UrFe^{II}–CO$_2$H]$^-$** species with a characteristic UV-Vis absorption maximum at 439 nm and rR marker bands at ν_4 = 1347 cm^{-1}, ν_2 = 1545 cm^{-1}, ν_{Fe-C} = 436 cm^{-1}, ν_{C-OH} = 1109 cm^{-1} and infrared frequency at $\nu_{C=O}$ = 1679 cm^{-1}. The last proton transfer to **[UrFe^{II}–CO$_2$H]$^-$** (pK_a = 35) induces C–O bond cleavage (Figure S12) and releases a water molecule to form **UrFe^{II}–CO** observed as the single turnover product when a potential of –1.55 V *vs* Fc$^{+/0}$ was applied. The source of proton for this step could come from a water molecule or a bicarbonate trapped in the urea arms. Preliminary DFT calculations indicate that the N-H proton from the urea cannot be transferred for the second protonation step.[30, 38] To regenerate the **UrFe^{I}** active species and restart the catalytic cycle, a potential just negative enough (–1.67 V *vs* Fc$^{+/0}$) to reduce **UrFe^{II}–CO** (reduction peak at –1.65 V *vs* Fc$^{+/0}$) is needed.

Conclusion

In this study, we report an original effect of multipoint hydrogen bonding urea functions embarked on an iron porphyrin catalyst for the selective CO_2 reduction to CO. As commonly advocated, second-coordination shell functions inspired from the active sites of enzymes have been introduced on ligand scaffolds of metal complexes to establish a hydrogen bonding network with the incoming substrate, acting as proton relays or providing an electrostatic interaction with reaction intermediates. We found here that a multipoint hydrogen bonding scheme may also shift the redox activation step from the well-admitted Fe(0) to the Fe(I) state. Collected EPR, Resonance Raman, FTIR and UV-Vis spectroscopies converged to a two-electron activation of CO_2 starting from the Fe(I) oxidation state leading after protonation to an Fe(III)–COOH species. The addition of an electron and a proton to the latter leads to the cleavage of a C–O bond with the loss of water molecule leaving behind an Fe(II)–CO species. Such a remarkable shift opens new lines of research in the design of molecular catalysts to reach low overpotentials to perform multi-electronic CO_2 reduction catalysis.

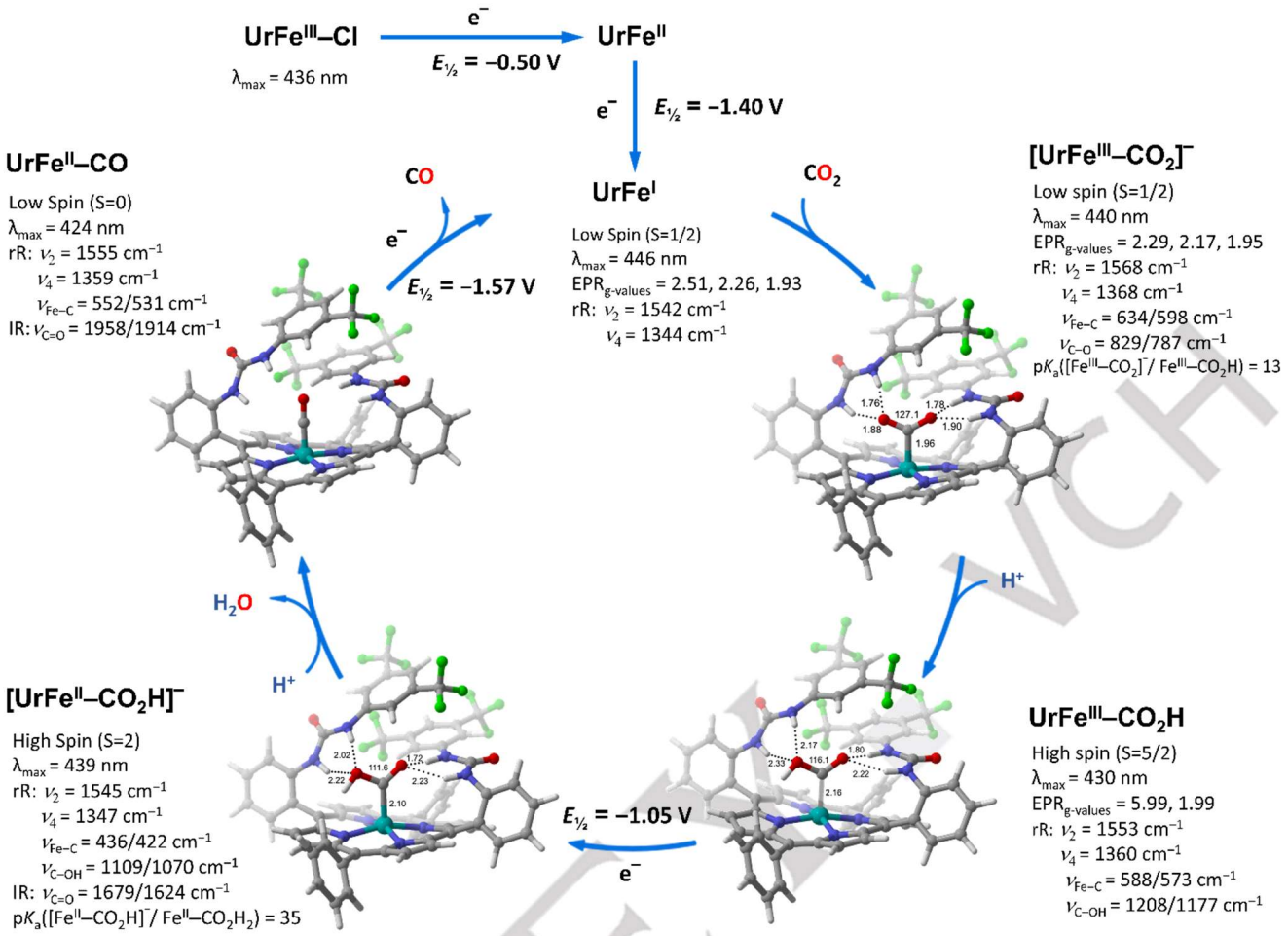

Scheme 2. Proposed mechanism for CO_2 reduction by **UrFe** catalyst at a potential less negative than that needed to reach Fe^0 oxidation state. Potential reported *vs* $Fc^{+/0}$. Isotope sensitive vibrations (using $^{13}CO_2$ or D_2O) are reported next to slash markers, see text for discussion.

Supporting Information

The authors have cited additional references within the Supporting Information.[44-50]

Acknowledgements

This work has been supported by the French National Research Agency (LOCO, grant N°: ANR-19-CE05-0020-02), and LABEX CHARMMMAT (grant N°: ANR-11-LABX-0039) and the French Infrastructure for Integrated Structural Biology (FRISBI, ANR-10-INSB-05-01). The computational studies were performed using HPC resources from GENCI (Grant 2022- A0130810977). We thank CNRS, CEA Saclay, ICMMO and University Paris-Saclay for the financial support. A.A. thanks Institut Universitaire de France for support.

Keywords: Iron Porphyrin • Carbon Dioxide • Electrocatalysis • Mechanism • Spectroscopy

[1] J. R. Botlton, D. O. Hall, in *Photochem. Photobiol., Vol. 53*, **1991**, pp. 545-548.
[2] J. Barber, A. V. Ruban, *Photosynthesis and Bioenergetics*, **2017**.
[3] M. Can, F. A. Armstrong, S. W. Ragsdale, *Chem Rev* **2014**, *114*, 4149-4174.
[4] M. I. Hoffert, K. Caldeira, A. K. Jain, E. F. Haites, L. D. D. Harvey, S. D. Potter, M. E. Schlesinger, S. H. Schneider, R. G. Watts, T. M. L. Wigley, D. J. Wuebbles, *Nature* **1998**, *395*, 881-884.
[5] F. Franco, C. Rettenmaier, H. S. Jeon, B. Roldan Cuenya, *Chem. Soc. Rev.* **2020**, *49*, 6884-6946.
[6] Z. Liang, H.-Y. Wang, H. Zheng, W. Zhang, R. Cao, *Chem. Soc. Rev.* **2021**, *50*, 2540-2581.
[7] E. Boutin, M. Robert, *Trends in Chemistry* **2021**, *3*, 359-372.
[8] S. Amanullah, P. Saha, A. Nayek, M. E. Ahmed, A. Dey, *Chem. Soc. Rev.* **2021**, *50*, 3755-3823.
[9] E. Boutin, L. Merakeb, B. Ma, B. Boudy, M. Wang, J. Bonin, E. Anxolabehere-Mallart, M. Robert, *Chem. Soc. Rev.* **2020**, *49*, 5772-5809.
[10] D. G. Nocera, *Acc. Chem. Res.* **2017**, *50*, 616-619.

[11] Z. W. Seh, J. Kibsgaard, C. F. Dickens, I. Chorkendorff, J. K. Norskov, T. F. Jaramillo, *Science* **2017**, *355*, eaad4998.
[12] Z. Guo, G. Chen, C. Cometto, B. Ma, H. Zhao, T. Groizard, L. Chen, H. Fan, W.-L. Man, S.-M. Yiu, K.-C. Lau, T.-C. Lau, M. Robert, *Nature Catalysis* **2019**, *2*, 801-808.
[13] P. Saha, S. Amanullah, A. Dey, *Acc. Chem. Res.* **2022**, *55*, 134-144.
[14] D. Xu, K. Li, B. Jia, W. Sun, W. Zhang, X. Liu, T. Ma, *Carbon Energy* **2022**, *5*, e230.
[15] J. Wang, S. Dou, X. Wang, *Sci Adv* **2021**, *7*.
[16] M. E. Ahmed, S. Adam, D. Saha, J. Fize, V. Artero, A. Dey, C. Duboc, *Acs Energy Lett* **2020**, *5*, 3837-3842.
[17] E. Nichols, J. S. Derrick, S. K. Nistanaki, P. T. Smith, C. J. Chang, *Chem. Sci.* **2018**, *9*, 2952-2960.
[18] E. A. Mohamed, Z. N. Zahran, Y. Naruta, *Chem. Commun.* **2015**, *51*, 16900-16903.
[19] C. Zhang, P. Gotico, R. Guillot, D. Dragoe, W. Leibl, Z. Halime, A. Aukauloo, *Angew Chem Int Ed* **2023**, *62*, e202214665.
[20] C. G. Margarit, C. Schnedermann, N. G. Asimow, D. G. Nocera, *Organometallics* **2019**, *38*, 1219-1223.
[21] M. W. Drover, *Chem. Soc. Rev.* **2022**, *51*, 1861-1880.
[22] T. Ouyang, H. J. Wang, H. H. Huang, J. W. Wang, S. Guo, W. J. Liu, D. C. Zhong, T. B. Lu, *Angew. Chem. Int. Ed. Engl.* **2018**, *57*, 16480-16485.
[23] P. L. Cheung, S. C. Kapper, T. Zeng, M. E. Thompson, C. P. Kubiak, *J. Am. Chem. Soc.* **2019**, *141*, 14961-14965.
[24] P. T. Smith, E. M. Nichols, Z. Cao, C. J. Chang, *Acc. Chem. Res.* **2020**, *53*, 575-587.
[25] Y. Wu, Z. Jiang, X. Lu, Y. Liang, H. Wang, *Nature* **2019**, *575*, 639-642.
[26] J. W. Wang, L. Jiang, H. H. Huang, Z. Han, G. Ouyang, *Nat Commun* **2021**, *12*, 4276.
[27] A. Call, M. Cibian, K. Yamamoto, T. Nakazono, K. Yamauchi, K. Sakai, *ACS Catalysis* **2019**, *9*, 4867-4874.
[28] X. Zhang, M. Cibian, A. Call, K. Yamauchi, K. Sakai, *ACS Catalysis* **2019**, *9*, 11263-11273.
[29] P. Gotico, Z. Halime, A. Aukauloo, *Dalton Trans* **2020**, *49*, 2381-2396.
[30] P. Gotico, B. Boitrel, R. Guillot, M. Sircoglou, A. Quaranta, Z. Halime, W. Leibl, A. Aukauloo, *Angew Chem Int Ed* **2019**, *58*, 4504-4509.
[31] P. Gotico, L. Roupnel, R. Guillot, M. Sircoglou, W. Leibl, Z. Halime, A. Aukauloo, *Angew Chem Int Ed* **2020**, *59*, 22451-22455.
[32] E. Pugliese, P. Gotico, I. Wehrung, B. Boitrel, A. Quaranta, M. H. Ha-Thi, T. Pino, M. Sircoglou, W. Leibl, Z. Halime, A. Aukauloo, *Angew Chem Int Ed* **2022**, *61*, e202117530.
[33] K. M. Vogel, P. M. Kozlowski, M. Z. Zgierski, T. G. Spiro, *Inorg. Chim. Acta* **2000**, *297*, 11-17.
[34] S. Amanullah, P. Saha, R. Saha, A. Dey, *Inorg. Chem.* **2019**, *58*, 152-164.
[35] C. Costentin, S. Drouet, G. Passard, M. Robert, J. M. Saveant, *J. Am. Chem. Soc.* **2013**, *135*, 9023-9031.
[36] S. Amanullah, P. Saha, A. Dey, *J. Am. Chem. Soc.* **2021**, *143*, 13579-13592.
[37] R. J. Donohoe, M. Atamian, D. F. Bocian, *J. Am. Chem. Soc.* **1987**, *109*, 5593-5599.
[38] J. S. Derrick, M. Loipersberger, S. K. Nistanaki, A. V. Rothweiler, M. Head-Gordon, E. M. Nichols, C. J. Chang, *J. Am. Chem. Soc.* **2022**, *144*, 11656-11663.
[39] Y. Matsubara, *Acs Energy Lett* **2019**, *4*, 1999-2004.
[40] J. M. Burke, J. R. Kincaid, S. Peters, R. R. Gagne, J. P. Collman, T. G. Spiro, *J. Am. Chem. Soc.* **1978**, *100*, 6083-6088.
[41] C. Romelt, S. Ye, E. Bill, T. Weyhermuller, M. van Gastel, F. Neese, *Inorg. Chem.* **2018**, *57*, 2141-2148.
[42] P. A. Davethu, S. P. de Visser, *J. Phys. Chem. A* **2019**, *123*, 6527-6535.
[43] B. Mondal, A. Rana, P. Sen, A. Dey, *J. Am. Chem. Soc.* **2015**, *137*, 11214-11217.
[44] M. J. Frisch, G. W. Trucks, H. B. Schlegel, G. E. Scuseria, M. A. Robb, J. R. Cheeseman, G. Scalmani, V. Barone, B. Mennucci, G. A. Petersson, H. Nakatsuji, M. Caricato, X. Li, H. P. Hratchian, A. F. Izmaylov, J. Bloino, G. Zheng, J. L. Sonnenberg, M. Hada, M. Ehara, K. Toyota, R. Fukuda, J. Hasegawa, M. Ishida, T. Nakajima, Y. Honda, O. Kitao, H. Nakai, T. Vreven, J. A. Montgomery Jr., J. E. Peralta, F. Ogliaro, M. Bearpark, J. J. Heyd, E. Brothers, K. N. Kudin, V. N. Staroverov, R. Kobayashi, J. Normand, K. Raghavachari, A. Rendell, J. C. Burant, S. S. Iyengar, J. Tomasi, M. Cossi, N. Rega, J. M. Millam, M. Klene, J. E. Knox, J. B. Cross, V. Bakken, C. Adamo, J. Jaramillo, R. Gomperts, R. E. Stratmann, O. Yazyev, A. J. Austin, R. Cammi, C. Pomelli, J. W. Ochterski, R. L. Martin, K. Morokuma, V. G. Zakrzewski, G. A. Voth, P. Salvador, J. J. Dannenberg, S. Dapprich, A. D. Daniels, Ol . Farkas, J. B. Foresman, J. V. Ortiz, J. Cioslowski, D. J. Fox, Gaussian 09, revision A.01; Gaussian, Inc: Wallingford, CT, 2009., M. J. Frisch, G. W. Trucks, H. B. Schlegel, G. E. Scuseria,M. A. Robb, J. R. Cheeseman, G. Scalmani, V. Barone,G. A. Petersson, H. Nakatsuji, X. Li, M. Caricato, A. V. Marenich, J. Bloino, B. G. Janesko, R. Gomperts, B. Mennucci, H. P. Hratchian,J. V. Ortiz, A. F. Izmaylov, J. L. Sonnenberg, D. Williams- Young, F. Ding, F. Lipparini, F. Egidi, J. Goings, B. Peng, A. Petrone,T. Henderson, D. Ranasinghe, V. G. Zakrzewski, J. Gao, N. Rega,G. Zheng, W. Liang, M. Hada, M. Ehara, K. Toyota, R. Fukuda,J. Hasegawa, M. Ishida, T. Nakajima, Y. Honda, O. Kitao, H. Nakai,T. Vreven, K. Throssell, J. A. Montgomery, Jr., J. E. Peralta, F. Ogliaro, M. J. Bearpark, J. J. Heyd, E. N. Brothers, K. N. Kudin, V. N. Staroverov, T. A. Keith, R. Kobayashi, J. Normand, K. Raghavachari, A. P. Rendell, J. C. Burant, S. S. Iyengar, J. Tomasi, M. Cossi, J. M. Millam, M. Klene, C. Adamo, R. Cammi,J. W. Ochterski, R. L. Martin, K. Morokuma, O. Farkas, J. B. Foresman, and D. J. Fox, Gaussian, Inc., Wallingford CT, 2016. Gaussian 16, Revision B.01.
[45] S. Grimme, S. Ehrlich, L. Goerigk, *J. Comput. Chem.* **2011**, *32*, 1456–1465.
[46] A. D. Becke, *J. Chem. Phys.*, **1993**, *98*, 5648-52.
[47] F. Weigend and R. Ahlrichs *Phys. Chem. Chem. Phys.*, **2005**, *7*, 3297-305.
[48] a) V. Barone, M. Cossi *J. Phys. Chem. A* **1998**, *102*, 11, 1995–2001; b) M. Cossi, N. Rega, G. Scalmani, and V. Barone, *J. Comp. Chem.*, **2003**, *24,* 669-81.
[49] J.-D. Chai, M. Head-Gordon, *Phys. Chem. Chem. Phys.* **2008**, *10*, 6615–6620.
[50] A. Malloum, J. Conradie, *J. Mol. Liq.* **2021**, *335*, 116032.

Entry for the Table of Contents

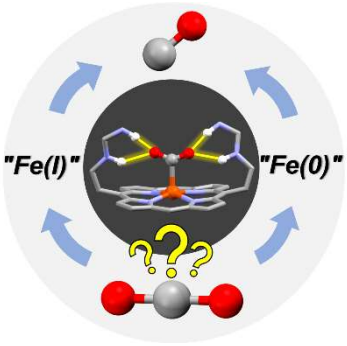

Bio-inspired second coordination sphere inducing a multipoint hydrogen bonding network triggers CO_2 activation at an earlier stage of the reaction mechanism in CO_2-to-CO electrocatalytic reduction by an iron porphyrin catalyst. Electrochemical and comprehensive spectroscopic investigations supported by DFT calculations revealed an unprecedented change in the active species' formal oxidation state from Fe(0) to Fe(I).

Institute and/or researcher Twitter usernames: @ICMMO-UMR8182